Chiral Recognition among Tris(diimine)−Metal Complexes. 4. Atomistic Computer Modeling of a Monolayer of $[Ru(bpy)_3]^{2+}$ Intercalated into a Smectite Clay[1]

Josef Breu*

Institut für Anorganische Chemie der Universität Regensburg, D-93040 Regensburg, Germany

C. Richard A. Catlow

Davy Faraday Research Laboratory, 21 Albemarle Street, London W1X 4BS, U.K.

Received February 3, 1995[⊗]

Lattice energy minimization techniques have been used to study the 2D-molecular organization of a monolayer of $[Ru(bpy)_3]^{2+}$ confined between two clay layers with respect to the stereochemistry of the guest complexes. The simulation results show the importance of both host−guest and guest−guest interactions in determining the structure of the interlamellar space. In the two structures with the lowest energy there is a perfect fit between guest shape and corrugation of the clay surfaces, while the lateral interactions between complex cations are favorable. The lattice energy minimum is observed with different 2D-arrangements of complex cations for an enantiomeric and a racemic monolayer. On the basis of this result the reported effect of chirality on the adsorption capacity can be rationalized.

1. Introduction

The packing of molecules in the solid state has a crucial effect on the properties of the resulting material. However, supramolecular synthesis, or the control of molecular orientation in the condensed phase, is an extremely difficult problem.[2]

Over the last 30 or 40 years a great deal of progress has been achieved in understanding the intermolecular interactions of organic molecules in the context of crystal packing.[2,3] But there have been few attempts to model the packing modes of inorganic and organometallic molecular compounds[4−7] and salts.[8−11]

Only recently have investigators begun to take advantage of the 2-dimensionally-ordered framework of intercalation hosts to control chemical interactions at the supramolecular level.[12] Here the template is a layered inorganic host, e.g. a clay, that accommodates guest molecules in specific orientations, at certain distances.

Clays are hydrous aluminosilicates with layer structures and belong to the larger group of phyllosilicates of which micas are probably the most widely known. The essential features of phyllosilicate structures are the continuous two-dimensional tetrahydral M_2O_5 ($M = Si^{4+}, Al^{3+}$) sheets, the basal oxygens of which are arranged in a Kagomé lattice and form a hexagonal (in ideal configuration) mesh pattern (Figure 1b). For the so-called 2:1 class, of which micas and smectites are members, two tetrahedral sheets are linked via the apical oxygen by an edge-sharing octahedral sheet, $M'O_4(OH)_2$ ($M = Al^{3+}, Mg^{2+}, Li^{+}$), and both surfaces of the silicate layer consist of the hexagonal mesh of basal oxygens (Figure 1a). Hence the clay surfaces show some corrugation, and there is a triangular lattice of

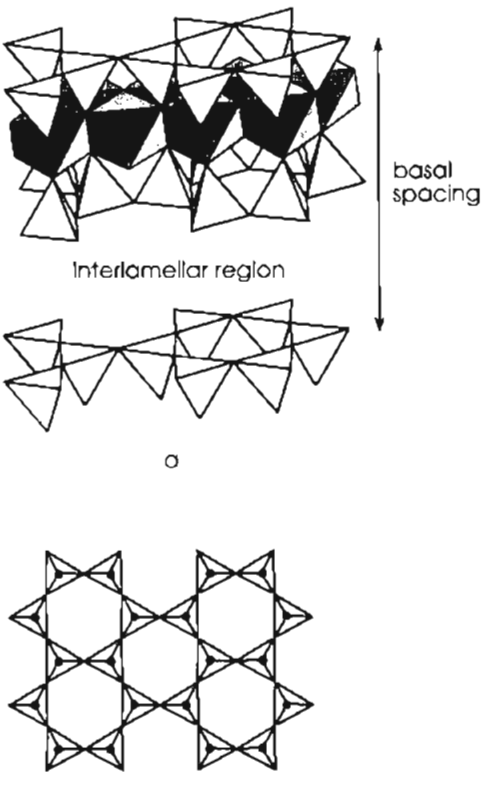

Figure 1. (a) Schematic illustration of the crystal structure of trioctahedral 2:1 phyllosilicates showing the basal spacing ($c^{\perp}_{exp}$). (b) Tetrahedral sheet viewed perpendicular to the silicate layer.

[⊗] Abstract published in *Advance ACS Abstracts*, July 15, 1995.

(1) Breu, J.; Range, K.-J. *Monatsh. Chem.* **1994**, *125*, 153.
(2) Desiraju, G. R. *Crystal Engineering*; Materials Science Monographs; Elsevier: Amsterdam, 1989.
(3) Kitaigorodski, A. I. *Molekülkristalle*; Akademie-Verlag: Berlin, 1979.
(4) Braga, D.; Grepioni, F.; Sabatino, P. *J. Chem. Soc., Dalton Trans.* **1990**, 3137.
(5) Braga, D.; Grepioni, F. *Organometallics* **1992**, *11*, 711.
(6) Braga, D.; Grepioni, F.; Sabatino, P.; Gavezzotti, A. *J. Chem. Soc., Dalton Trans.* **1992**, 1185.
(7) Braga, D.; Grepioni, F. *Acc. Chem. Res.* **1994**, *27*, 51.
(8) Müller, U. *Acta Crystallogr., Sect. B* **1980**, *36*, 1075.
(9) Braga, D.; Grepioni, F. *Organometallics* **1992**, *11*, 1256.
(10) Mingos, D. M. P.; Rohl, A. L. *J. Chem. Soc., Dalton Trans.* **1991**, 3419.
(11) Rohl, A. L.; Mingos, D. M. P. *J. Chem. Soc., Dalton Trans.* **1992**, 3541.
(12) Bein, T., Ed. *Supramolecular Architecture, Synthetic Control in Thin Films and Solids*; ACS Symposium Series; American Chemical Society: Washington, DC, 1992.

0020-1669/95/1334-4504$09.00/0

hollows into which interlamellar guests may protrude. In smectites, the silicate layers typically bear a net charge of 0.2–0.6 e^- per $O_{10}(OH)_2$ formula unit. Charge balance in natural smectites is maintained by hydrated cations in the interlamellar space. Because of the medium layer charge, smectite clays possess a combination of cation exchange, intercalation, intersalation (accommodation of ion pairs into the interlamellar region), and swelling properties which makes them unique.

In clay intercalation compounds (CIC's), the host layers are highly rigid towards transverse distortion and have been classified as class III layered solids according to the scheme established by Solin.[13] Clays therefore provide an ideal system to study molecular recognition in 2D-assemblies of cations confined between corrugated surfaces, the minimum energy structure being the balance between different host–guest and guest–guest interactions.

With chiral tris(1,10-phenanthroline)– or tris(2,2′-bipyridyl)–metal complexes ($[M(phen)_3]^{n+}$, $[M(bpy)_3]^{n+}$, M = Fe^{2+},Ru^{2+}, Ni^{2+}) as guest molecules, remarkable chiral recognition phenomena have been observed.[14–17] For example the adsorption capacities differ by a factor of ≈2 depending on whether the complexes are added as a racemic mixture or as a pure enantiomer. However, since clay minerals are achiral, there is no simple explanation for the underlying chiral recognition mechanism.

Chiral recognition and discrimination is a distinctive property of dissymmetric molecules. An analysis of the packing of dissymmetric molecules requires explicit consideration of the finite size, shape, and electrostatic potential and the particular stereochemistry in relation to their separation and relative orientation.[18–20]

But, because smectites and their intercalation compounds are microcrystalline and poorly ordered in the crystallographic sense, it is notoriously difficult to ascertain by direct experiment the atomic detail of the interlamellar region. For such systems, computer simulations can provide valuable information.[21–23] We have therefore performed atomistic simulations for a monolayer of $[Ru(bpy)_3]^{2+}$ intercalated in a trioctahedral smectite with a layer charge originating from the tetrahedral sheets (saponite), $\{[Mg_3]^{oct}[Si_{3.5}Al_{0.5}]^{tet}O_{10}(OH)_2\}^{-0.5}$. Our main objective was to gain insight into the basic effects governing the 2D molecular organization as modified by the peculiar anion clay, especially with respect to the stereochemistry of the guest complexes.

2. Computational Methods

Modeling the packing of complex cations within the microenvironment of the interlamellar space requires a sound treatment of both long-range electrostatic interactions and the short range interactions between guest molecules and between guests and the host lattice. This was achieved in the present study with a classical description of the intracrystalline forces based on the Born model; a covalent "molecular mechanics" potential was used to model the intramolecular forces, while atom–atom pair potentials described the lattice–molecule and molecule–molecule interactions.

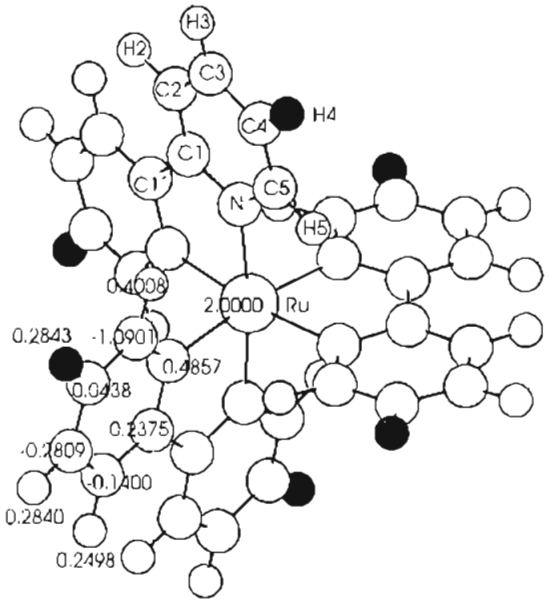

Figure 2. ORTEP diagram of $[Ru(bpy)_3]^{2+}$ viewed along its C_3 axis showing the atom labeling scheme and potential-derived partial charges. The protruding Hydrogen atoms are marked.

We used the method of so–called lattice energy minimization with periodic boundary condition, which takes a starting structure and a set of interatomic potentials and calculates the structure corresponding to the nearest energy minimum.[22–26] The lattice energy was calculated by standard summation procedures, using the Ewald method[27] (rather than simple truncation) for evaluation of the electrostatic term, and real space summation for the short range components of the interaction. Since entropy effects are not considered, the treatment simulates the behavior at 0 K, although within the context of the quasi-harmonic approximation higher temperature structures and properties may be investigated using temperature dependent lattice parameters.

A comparison of crystal structures of hexafluorophosphate salts of $[Ru(bpy)_3]^{2+}$, $[Ru(bpym)_3]^{2+}$, and $[Ru(bpz)_3]^{2+}$ (bpym = 2,2′-bipyrimidine, bpz = 2,2′-bipyrazine) shows that replacement of C by N in the aromatic ring causes little variation in the molecular structures of the complex cations.[28–30] However, the variation in the molecular electrostatic potential (MEP) induces completely different crystal packings especially in respect to chiral recognition in the crystal.[31] For instance, while $[Ru(bpy)_3]^{2+}$ is built up by homochiral layers, $[Ru(bpym)_3]^{2+}$ consists of racemic layers. Therefore special attention was paid to the procedures used in handling the long-range Coulombic interactions between atoms on separate complexes and on the host.

The MEP of the complexes was represented by point charges positioned at the nucleus of the atoms. The point charges were fitted to the MEP with the program RATTLER.[32] The charge of the central atom was fixed and symmetry-equivalent atoms were constrained or averaged to give the same charges (Figure 2). The MEP was calculated from the molecular wave functions which were computed ab initio with

(13) Solin, S. A. *J. Mol. Catal.* **1984**, *27*, 293.
(14) Yamagishi, A.; Soma, M. *J. Am. Chem. Soc.* **1981**, *103*, 4640.
(15) Yamagishi, A. In *Dynamic Processes on Solid Surfaces*; Tamaru, K., Ed.; Plenum Press: New York, 1993.
(16) Villemure, G. *Clays Clay Miner.* **1990**, *38*, 623.
(17) Joshi, V.; Kotkar, D.; Ghosh, P. K. *Proc. Indian Acad. Sci. (Chem. Sci.)* **1990**, *102*, 203.
(18) Kuroda, R.; Mason, S. F.; Rodger, C. D.; Seal, R. H. *Mol. Phys.* **1981**, *42*, 33.
(19) Kuroda, R.; Biscarini, P. *J. Chem. Soc., Dalton Trans.* **1990**, 3393.
(20) Kuroda, R. *Inorg. Chem.* **1991**, *30*, 4954.
(21) Gale, J. D.; Cheetham, A. K.; Jackson, R. A.; Catlow, C. R. A.; Thomas, J. M. *Adv. Mater.* **1990**, 2, 487.
(22) Catlow, C. R. A. In *Computer Modeling of Fluids Polymers and Solids*; Catlow, C. R. A., Parker, S. C., Allen, M. P., Eds.; NATO ASI Series C; Kluwer Academic Publishers: Dordrecht, The Netherlands, 1990.
(23) Catlow, C. R. A.; Bell, R. G.; Gale, J. D. *J. Mater. Chem.* **1994**, *4*, 781.
(24) Catlow, C. R. A.; Cormack, A. N. *Int. Rev. Phys. Chem.* **1987**, *6*, 227.
(25) Collins, D. R.; Catlow, C. R. A. *Amer. Mineral.* **1992**, *77*, 1172.
(26) Collins, D. R.; Catlow, C. R. A. *Mol. Simulat.* **1990**, *4*, 341.
(27) Ewald, P. P. *Ann. Phys. (Leipzig)* **1921**, *64*, 253.
(28) Lai, H.; Jones, D. S.; Schwind, D. C.; Rillema, D. P. *J. Cryst. Spectrosc. Res.* **1990**, *20*, 321.
(29) Rillema, D. P.; Jones, D. J. *J. Chem. Soc., Chem. Commun.* **1979**, 849.
(30) Rillema, D. P.; Jones, D. S.; Woods, C.; Levy, H. A. *Inorg. Chem.* **1992**, *31*, 2935.
(31) Breu, J.; Range, K.-J. *Monatsh. Chem.* **1994**, *125*, 141.
(32) Reynolds, C. A.; Ferenczy, G. G. *Academic version of RATTLER*; Oxford Molecular: Magdalen Centre, Oxford Science Park, Sandford on Thames, Oxford, U.K., 1993.

density functional methods.[33] In deriving net atomic charges from the MEP strange values may result especially for well-buried atoms far from the surface; however they reproduce the total electrostatic potential on the surface quite well and are still the best for studying intermolecular interactions.[34]

For the clay, ionic model potentials with formal charges on Si, Mg, and O and a shell model treatment of the polarisability of the oxygen atom were used. Since the distribution of Al and Si in the tetrahedral sites generally shows no long-range ordering, we continued to use a hybrid species ($Al_{0.125}Si_{0.875}$) of charge +3.875. The remainder of the force field used to present the silicate framework was successfully employed for micas previously and is described in detail elsewhere.[25,26]

The molecular geometry of the complexes was preservered at that found in the crystal structure of $[Ru(bpy)_3](PF_6)_2$[29,30] by using strong harmonic potentials between the atoms to fix the bond length and three-body potentials to fix the bond angles. We note that reliable force field parameters are unavailable for the Ru−N interactions. Moreover, while there is little diviation in the molecular structures of simular complexes like $[Ru(bpy)_3]^{2+}$, $[Ru(bpym)_3]^{2+}$, and $[Ru(bpz)_3]^{2+}$,[28−30] variation of the bond and angle parameters would have increased the complexity of the calculation while having little effect on the results. However, since the torsional angle around the C1−C1′ bond shows some variation in crystal structures, energy terms from the consistent valence forcefield (cvff)[35] were taken to model torsional motions.

Nonbonding interactions between the complex cations, and both the framework and adjacent complexes are represented using Buckingham potentials fitted by Oie et al.[36] to a large sample of organic crystal structures. These parameters have been supplemented by MM2-Lennard-Jones potentials[37] for the Si−C and Si−$H_{complex\ cation}$ interactions. The cut-off distance for the nonbonding terms was 16 Å. Ru−Ru, Ru−framework, as well as octahedral cation−complex cation interactions were neglected.

In common with many zeolite simulations it is not reasonable to suppose that the host is unperturbed; instead, the silicate framework must be allowed to relax simultaneously during the minimization. In particular, the interlayer spacing and the relative shift of the silicate layers must be allowed to alter; hence, the shape of the unit cell is variable during minimization.

3. Choice of Unit Cell

Since the only experimental structural information for the CIC under investigation is the basal spacing derived from powder diffraction at room temperature ($c^{\perp}_{exp}$ = 17.9 Å),[38] making a sensible choice for the unit cell and sampling enough configurational space are the most severe problems in simulation.

3.1. Size. To be able to model a racemically packed structure we need a minimum of two complex molecules in the unit cell. The area covered by two trischelate complexes of the above mentioned ligands in two-dimensional packings is between 150−200 Å^2.[29,31,39−41] The shortest separation between complexes of the same chirality in $[Ru(bpy)_3](PF_6)_2$ [29,30] and $[Fe(phen)_3]I_2{\cdot}2H_2O$[41] is 10.6 Å.

On the basis of these three requirements, we chose a 2*a*2*b* supercell of the mica phlogopite with space symmetry reduced to *P*1 (*a* = 10.632 Å, *b* = 18.442 Å).[42] The charge of the hybrid tetrahedral cation was adjusted to provide electroneutrality, and the layer charge of the saponite (0.5 e^- per $O_{10}(OH)_2$ formula unit) is therefore at the high end for smectites. This cell provides a basal area of 196.1 Å^2 and the shortest axis, and hence the repeat distance for complexes of the same chirality, is 10.6 Å.

3.2. Shape. The shape of the unit cell was chosen based on Monte Carlo results recently published by Sato and co-workers.[43−46]

$Ru(bpy)_3^{2+}$ shows D_3 symmetry with a trigonal distorted octahedral coordination sphere. Along the C_3 axis three hydrogen atoms each protrude above and below the molecule (H4, marked in Figure 2). Their relative position is an extension of the central coordination. They are arranged in two trigonal planes, which in turn form a trigonal distorted octahedron. The hydrogens in the triangles are 6.2 Å apart.

The hexagonal hollows on the clay surface are 5.3 Å apart. So there is a fairly good match between the surface structure of the clay and the shape of complexes.

The Monte Carlo results suggest that the favorable host−guest interaction is with complexes aligned with their C_3 axis perpendicular to the silicate surface and the peripheral hydrogens sticking into the hollows.

However, the arrangement of the top and bottom hydrogen triangle is a projection of the octahedral coordination. As upper and lower tetrahedral sheets have to be shifted by *a*/3 in 1 M micas as a direct consequence of interfacing two tetrahedral sheets to an octahedral sheet, so the two clay layers between which the complexes are sandwiched have to be shifted relative to each other to put both the upper and lower hydrogen triple above hollows (Figure 3). Therefore the angles of the triclinic unit cell were chosen to provide these shifts and the initial c-axis was adjusted to give the experimentally observed basal spacing ($c^{\perp}_{exp}$ = 17.9 Å).

Since the basal area of the 2*a*2*b* supercell of phlogopite provides eight hexagonal hollows, the above assumptions lead to four different packing patterns for enantiomeric and racemic layers of complex cations each (Figure 3). These arrangements differ in the relative positions and distances of the cations. Because of geometrical constraints for patterns 3 and 4 with trigonal hydrogen faces pointing in different directions, only 9 out of the 12 peripheral hydrogens in the unit cell can be arranged above hollows. All configurations have been taken as starting points for energy minimization in order to identify the associated local minima. The minimizations have been performed at constant pressure allowing all atomic coordinates and the unit cell dimensions to relax. The calculation employed the recently developed GULP code,[47] which uses standard methods, including the Ewald summation,[27] to undertake lattice energy calculations and minimizations.

4. Results and Discussion

The resulting lattice energies and lattice parameters are given in Table 1. As expected, there is little correlation between density, volume, basal spacing, and the total lattice energy, because the energy is a complex functional of different host−guest and guest−guest interactions.

The dimensions of *a*, *b*, and γ stay close to the experimental data for phlogopite used as starting values (10.632 Å, 18.442

(33) Daul, C.; Baerends, E. J.; Vernooijs, P. *Inorg. Chem.* **1994**, *33*, 3538.
(34) Reynolds, C. A.; Ferenczy, G. G.; Richards, W. G. *J. Mol. Struct.* **1992**, *256*, 249.
(35) *Molecular Simulation Program DISCOVER*; BIOSYM Technologies: San Diego, CA, 1993.
(36) Oie, T.; Maggiora, G. M.; Christoffersen, R. E.; Duchamp, D. J. *Int. J. Quantum Chem. Quantum Biol. Symp.* **1981**, *8*, 1.
(37) Nicholas, J. B.; Trouw, F. R.; Mertz, J. E.; Iton, L. E.; Hopfinger, A. J. *J. Phys. Chem.* **1993**, *97*, 4149.
(38) Villemure, G. *Clays Clay Miner.* **1991**, *39*, 580.
(39) Wada, A.; Katayama, C.; Tanaka, J. *Acta Crystallogr., Sect. B* **1976**, *32*, 1121.
(40) Harrowfield, J. M.; Sobolev, A. N. *Aust. J. Chem.* **1994**, *47*, 763.
(41) Johansson, L.; Molund, M.; Oskarsson, A. *Inorg. Chim. Acta* **1978**, *31*, 117.
(42) Knurr, R. A.; Bailey, S. W. *Clays Clay Miner.* **1986**, *34*, 7.
(43) Sato, H.; Yamagishi, A.; Kato, S. *J. Am. Chem. Soc.* **1992**, *114*, 10933.
(44) Sato, H.; Yamagishi, A.; Kato, S. *J. Phys. Chem.* **1992**, *96*, 9382.
(45) Sato, H.; Yamagishi, A.; Kato, S. *J. Phys. Chem.* **1992**, *96*, 9377.
(46) Sato, H.; Yamagishi, A.; Kato, S. *Clay Sci.* **1991**, *8*, 147.
(47) Gale, J.; *GULP. General utility lattice program*; Imperial College, London, U.K., 1993.

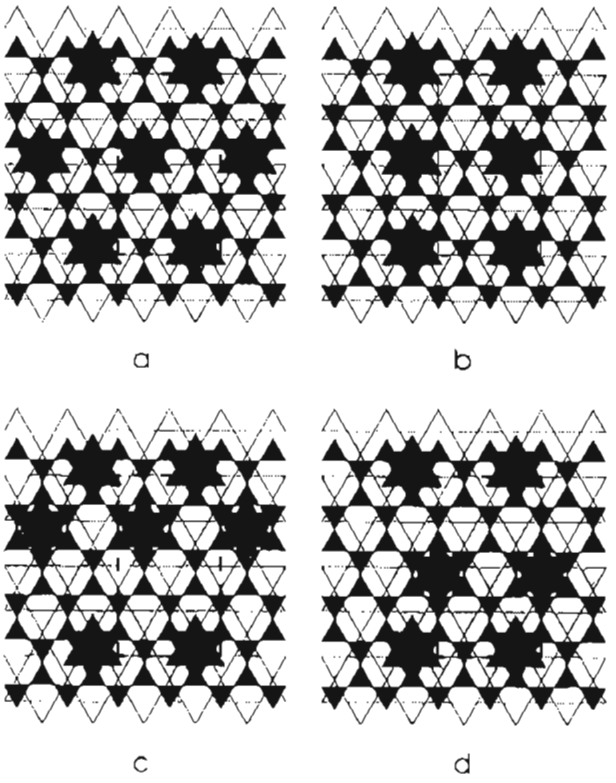

Figure 3. Schematic representation of the four packing configurations used as starting points for lattice energy minimization showing the match between guest shape and corrugation of the two silicate layers confining the interlamellar region: (a) pattern 1; (b) pattern 2; (c) pattern 3; (d) pattern 4. Dashed line = projection of the unit cell.

Å, 90.0°). The rigidity of the silicate layer is correctly preserved by the model even with such large pillars in the interlamellar space. However, c, α, and β and hence the basal spacing and relative shift of the two clay layers confining the interlamellar space vary considerably (also expressed as Δa and Δb in Table 1).

The guest complexes in patterns 3 and 4 move considerably from the initial position to the minimum, because there are large repulsive nonbonding interactions at the start and the host–guest interaction is not quite optimal. This, together with the variation in the shifts of upper and lower silicate layers, gives us some confidence that we have sampled a considerable amount of configurational space.

All calculated basal spacings are smaller than the experimental one ($c^{\perp}_{exp}$ = 17.9 Å). This trend was already observed for the mica simulations and is not surprising for a 0 K treatment.[25,26] Since the bonding in the clay layers is much stronger than that perpendicular to it, $c^{\perp}_{exp}$ is expected to increase more with temperature than a,b..

Of the huge number of CIC's which have been synthesized to date, there are relatively few examples for which the in-plane structure of the guest layers has been fully characterized.

If we neglect, in a first approximation, the effect of substrate corrugation, then we have a system of (2+) ions interacting via unscreened Coulomb interaction. The ground state structure of such a system is known to be a hexagonal lattice. The lattice constant of this is a function of the loading and hence of the charge density of the clay which is related to the cation exchange capacity (CEC) because of the charge-neutrality condition. Experimental backing for this model comes from adsorptive and diffusive properties of clay systems pillared with $[Cr(en)_3^{3+}]_x[Co(en)_2^{3+} - (en)]_{1-x}$ (en = ethylenediamine).[48] The formation of this incommensurate hexagonal lattice of pillars is also supported by an interpretation of the in-plane XRD peaks of smectites pillared with $[Ir(diamsar)]^{3+}$, $[Hg(diamsarH_2)]^{4+}$, and $[Hg(diamsar)]^{2+}$ (diamsar = 1,8-diamino-3,6,10,13,16,19-hexaazabicyclo[6.6.6]eicosane).[49]

On the other hand emission spectra show that (pyrenylbutyl)-trimethylammonium tends to cluster on the clay surface and is not adsorbed randomly.[50] Further, time-resolved luminescence studies on Δ,Λ-$[Ru(bpy)_3]^{2+*}$–hectorite have shown that these metal chelates aggregate within the clay matrix even at loading levels as low as 2 % of the CEC.[51] Moreover it was concluded that racemic $[Ru(bpy)_3]^{2+}$ is more aggregated than enantiomeric at low loadings.[52] These observations point toward a nonuniform distribution of adsorption sites on the clay surface (variation of the charge density in the plane of the silicate layer) or a strongly attractive lateral interaction of interlamellar guests.

The simulation results show that neither host–guest nor guest–guest interaction may be neglected for the system under consideration. For the two patterns with the lowest energy (enantiomeric pattern 1 and racemic pattern 2) there is a perfect fit between host and guest shape. All 12 peripheral hydrogens protrude into hexagonal hollows (Figures 4 and 5), emphasizing the importance of the host–guest interaction in determining the packing. The enantiomeric pattern 1 corresponds to the hexagonal lattice of point charges. However, it is coincidental that this 2D arrangement is commensurate with the host lattice at the chosen charge density.

The packing pattern for the enantiomeric minimum energy structure is almost indistinguishable from the two dimensional packing pattern realized in $[Ru(bpy)_3](PF_6)_2$[29,30] (Figure 6). This 2D lattice is clearly a valid minimum for enantiomeric layers. The model correctly reproduces the experimental fact that for certain mutual orientations and separations enantiomeric layers are energetically favorable with $[M(bpy)_3]^{n+}$ systems, even though this is not true in general (see below), as concluded from a literature review of crystal structures.[31]

The energy minimum for the racemic packing (Figure 7) does not correspond to the hexagonal pattern nor is it observed in any of the published crystal structures with common anions, lending further evidence to the distinct structure-modifying effect of the clay surface. While the mutual orientation and separation of the complexes with the same configuration along a is similar to enantiomeric pattern 1, the distance between complexes of the same chirality along b is shorter (9.3 Å), and the neighboring molecules penetrate each other, yielding a staggered parallel stacking of two bpy ligands. As a consequence of chirality, this penetration of two complexes approaching each other with parallel C_3 axis is only feasible with a racemic pair. Lateral interactions of this kind are one of the major motifs in crystal packings of polynuclear aromatic hydrocarbons[53] and should be favorable. The fact that racemic pattern 2 is the global minimum indicates that guest–guest interactions are important in determining the structure of the interlamellar space as well.

Our simulation assumes a perfect crystal. We are aware that clays and CIC's exhibit a wide variety of ordered, partially ordered and fully randomized c axis stacking arrangements. However, this affects only the interactions of guest species in different layers which is relatively long-range. Host–guest and

(48) Chen, B. Y.; Kim, H.; Mahanti, S. D.; Pinnavaia, T. J.; Cai, Z. X. *J. Chem. Phys.* **1994**, *100*, 3872.
(49) Tsvetkov, F.; White, J. *J. Am. Chem. Soc.* **1988**, *110*, 3183.
(50) Thomas, J. K. *Acc. Chem. Res.* **1988**, *21*, 275.
(51) Ghosh, P. K.; Bard, A. J. *J. Phys. Chem.* **1984**, *88*, 5519.
(52) Kamat, P. V.; Gopidas, K. R.; Mukherjee, T.; Johsi, V.; Kotkar, D.; Pathak, V. S.; Ghosh, P. K. *J. Phys. Chem.* **1991**, *95*, 10009.
(53) Desiraju, G. R.; Gavezzotti, A. *Acta Crystallogr., Sect. B* **1989**, *45*, 473.

Table 1

	pattern 1		pattern 2		pattern 3		pattern 4	
	enantiomeric	racemic	enantiomeric	racemic	enantiomeric	racemic	enantiomeric	racemic
tot. lattice energy (eV)	−4960.9597	−4960.2635	−4959.6444	−4961.4802	−4960.0786	−4960.4813	−4960.1044	−4960.7352
$E_{en} - E_{rac}$ (kJ/mol)	−67.174		177.130		38.903		60.864	
ΔE^a (kJ/mol)	50.221	117.395	177.130	0.0	135.236	96.381	132.746	71.883
a (Å)	10.729	10.710	10.753	10.727	10.733	10.735	10.733	10.728
b (Å)	18.602	18.616	18.617	18.596	18.580	18.590	18.578	18.591
c (Å)	18.770	18.877	18.891	18.724	20.695	18.804	18.475	18.676
α (deg)	70.69	70.85	70.26	70.95	62.79	71.33	75.51	71.51
β (deg)	79.11	79.66	79.43	79.07	73.65	79.43	77.64	79.02
γ (deg)	90.00	90.02	89.96	90.00	90.02	89.98	90.00	90.07
V (Å^3)	3463.8	3490.6	3491.3	3458.7	3481.3	3487.8	3478.3	3460.2
ϱ (g/cm^3)	2.001	1.986	1.985	2.004	1.991	1.987	1.993	2.003
$c^{\perp}$ (Å)	17.356	17.508	17.440	17.338	17.457	17.477	17.445	17.349
Δa (Å)	3.545	3.387	3.464	3.550	5.827	3.450	3.956	3.559
Δb (Å)	6.206	6.193	6.380	6.113	9.465	6.018	4.622	5.929

[a] Energy relative to the most stable configuration.

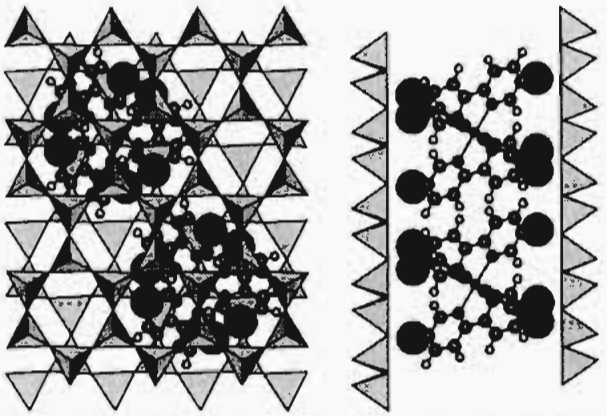

Figure 4. Structure (pattern 1) of the lattice energy minimum for an enantiomeric monolayer of $[Ru(bpy)_3]^{2+}$, intercalated in saponite, viewed perpendicular to the silicate layers (left) and along a (right). The protruding hydrogen atoms are marked and depicted with a real van der Waals radius.

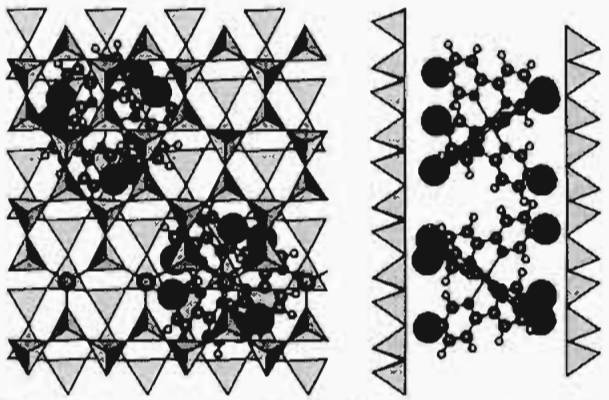

Figure 5. Structure (pattern 2) of the lattice energy minimum for a racemic monolayer of $[Ru(bpy)_3]^{2+}$, intercalated in saponite, viewed perpendicular to the silicate layers (left) and along a (right). The protruding Hydrogen atoms are marked and depicted with real van der Waals radius.

guest–guest interactions in the same layer are not directly affected by the long-range ordering in the third dimension.

For both enantiomeric and racemic packing minima, the complexes align with their C_3 axis perpendicular to the silicate layers. Both clay layers confining the interlamellar space simultaneously interact with the guest molecules which are located exactly in the middle. In all the other local minima with a less perfect guest–host fit, complexes are inclined to some degree.

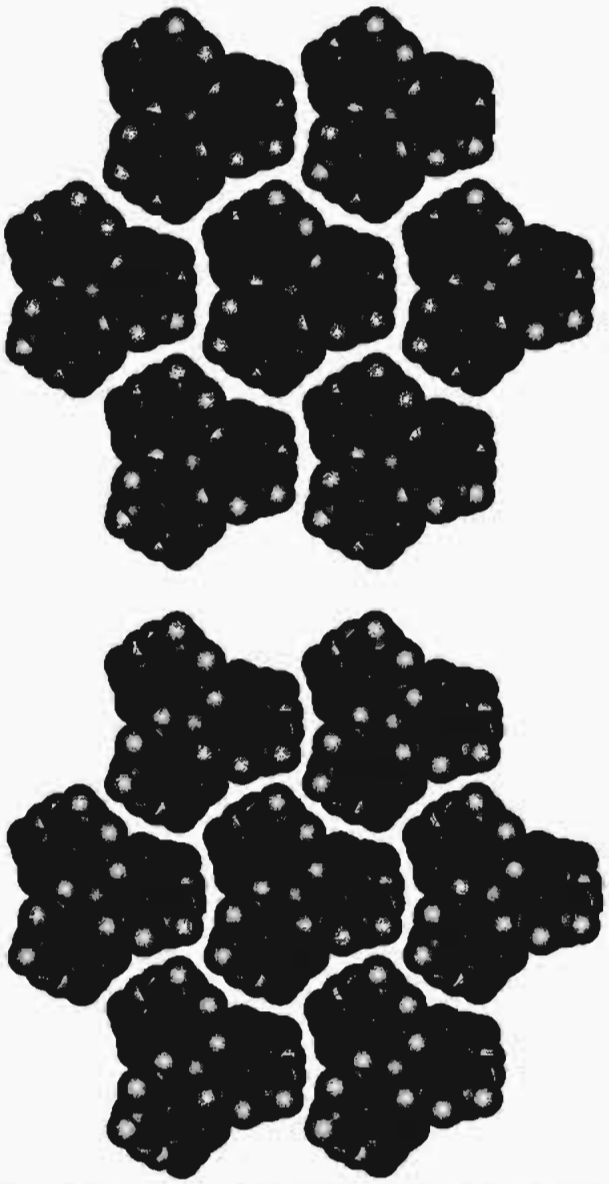

Figure 6. Space-filling model of the 2D-arrangement of $[Ru(bpy)_3]^{2+}$ in $[Ru(bpy)_3]$ $(PF_6)_2$[28,29] (top), and in the lattice energy minimum of enantiomeric $[Ru(bpy)_3]^{2+}$ intercalated in saponite (bottom).

We note that our calculations agree with earlier studies of Sato et al.[43–46] in so far as they found a perpendicular orientation of the C_3 axis of the complexes for the lowest energy configurations. It is, however, not possible to make a more

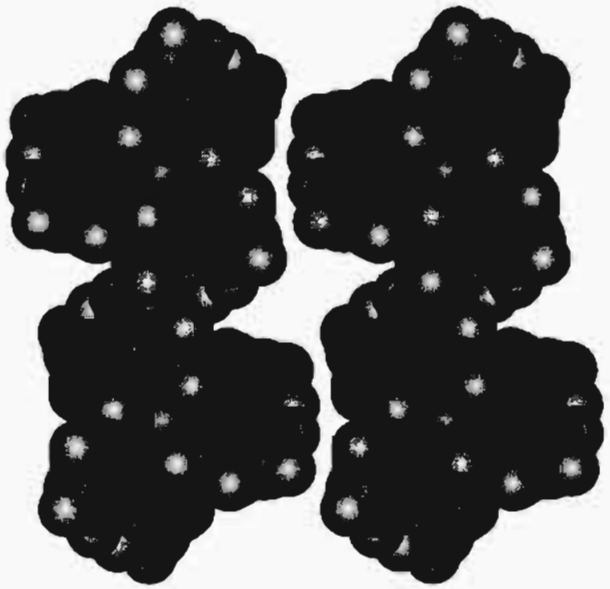

Figure 7. Space-filling model of the 2D-arrangement of $[Ru(bpy)_3]^{2+}$ in the lattice energy minimum of racemic $[Ru(bpy)_3]^{2+}$ intercalated in saponite.

detailed comparison with this earlier work which did not include the packing effects of 2D periodic arrays of complexes and did not allow the basal spacings and mutual displacements of upper and lower silicate sheet to vary simultaneously during the course of each simulation. Sato et al.[43,44] performed simulations for a pair of $[M(phen)_3]^{n+}$ or $[M(bpy)_3]^{n+}$ complexes in a box of 31.896 Å × 36.832 Å yielding a surface area of 587.8 Å^2 per complex molecule. Despite the rather low loading in respect to both charge density (0.57 e^- per $O_{10}(OH)_2$ unit) and available surface, they observed association of both enantiomeric and racemic pairs of $[M(phen)_3]^{n+}$ or $[M(bpy)_3]^{n+}$ in the simulation box. However, at this low surface loading the results of Sato et al. give only an indication of the molecular recognition process between a pair of guest molecules and the guest molecules and the host. Our simulations at high loading levels additionally explore the cooperative recognition and mutual reorientation that controls the assembling of larger 2D supramolecular arrays. In order to tackle the problem of whether or not pillars of the kind $[M(phen)_3]^{n+}$ or $[M(bpy)_3]^{n+}$ will at an intermediate loading aggregate to clusters in the interlamellar region of homogeneously charged smectites and what the structure of these clusters would be, rather large supercells will have to be employed, which will be a challenging task even to contemporary computer power.

The simulation results also offer an explanation for the observed effect of chirality on the adsorption capacity. In the case of $[Ru(bpy)_3]^{2+}$ the racemic mixture is adsorbed at levels within the CEC, while the enantiomer is adsorbed in 1.5−2.5-fold excess of the CEC.[16] According to XRD analysis,[38] the chelate forms a monomolecular layer at loadings less than 100% of the CEC, while at adsorption levels beyond the CEC, complex cations are arranged in a double-molecular layer. For charge neutrality, anions must also be incorporated in the interlamellar space in the latter case (Figure 8). For systems that are limited to monolayer adsorption, no difference is observed in the maximum adsorption amount between racemic and enantiomeric isomers.[1,54,55]

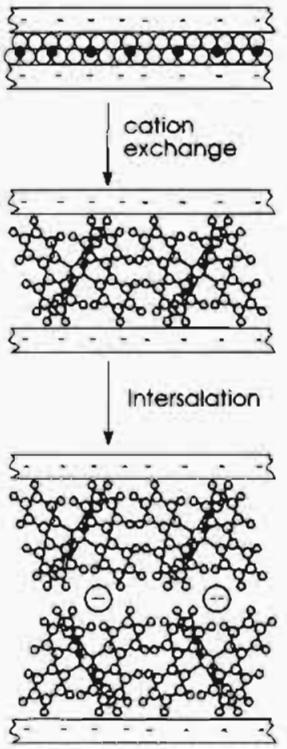

Figure 8. Schematic representation of the adsorption steps of $[Ru(bpy)_3]^{2+}$ into saponite.

Whether or not intersalation to the double-layer arrangement occurs for a given system is determined by the complex energetics of the intercalation reaction and the lowest energy packing for the monolayer in respect to ligand type and chirality.[31] The free energy paid by the further expansion of the basal spacing against the Coulombic attraction must be overcompensated by the energy gained by incorporating the second layer into the interlamellar space. Because complexes are strongly adsorbed, rearrangement of the monolayer is unlikely and the latter energy term is dependant on the structure of the monolayer. We find now that at the same packing density, the lowest energy for racemic layers and for enantiomeric layers of $[Ru(bpy)_3]^{2+}$, intercalated in a smectite, occurs with different structures (pattern 2 and pattern 1, respectively). We suggest that intersalation to the double-layer arrangement is energetically favorable only for the enantiomeric pattern. In $[Ru(bpy)_3](PF_6)_2$[29,30] (Figure 4) and in the homeotype $[Ni(bpdz)_3](ClO_4)_2$[56] (bpdz = 3,3′-bipyridazine) homochiral layers of the same type as the enantiomeric packing minimum are stacked on top of each other with the C_3 axis of the complex cations being collinear. In the latter, layers of the same chirality are stacked; layers of alternating chirality in the former. It shows that with this 2D lattice of complex cations double-molecular layers are energetically favorable, while the two-dimensional packing for the racemic minimum is not realised in any of the published crystal structures with common anions, and may be unique to the clay anion.

5. Conclusions

On the basis of these results we propose that the observed chiral recognition phenomena are founded in the lateral interactions between the guest complexes as modified by the corrugation of the silicate layer. The clay mineral controls the orientations and relative positions of the complex cations in the

(54) Kaneyoshi, M.; Yamagishi, A.; Taniguchi, M.; Aramata, A. *Clays Clay Miner.* **1993**, *41*, 1.
(55) Yamagishi, A.; Taniguchi, M.; Takahashi, M.; Asada, C.; Matsushita, N.; Sato, H. *J. Phys. Chem.* **1994**, *98*, 7555.
(56) Onggo, D.; Rae, A. D.; Goodwin, H. A. *Inorg. Chim. Acta* **1990**, *178*, 151.

interlamellar space based on the match between host and guest shapes.

But with this peculiar anion clay also a great deal may be learned about the basics of the packing of molecular ions in the solid state. This system illuminates the complex interplay of shape (also stereochemistry), nonbonding interactions, and molecular electrostatic potential in relation to separation and relative orientation in determining the packing of molecular ions in solids.

A more general implication of our results is that they demonstrate the detail and complexity of systems that may be investigated by contemporary computer modeling techniques, which may be used to probe energetics and structure of organometallic solids, and of materials of the type discussed here which include an interface between aluminosilicates and organometallics. As the use of such techniques becomes increasingly routine, they should find a growing use in addressing problems of the type considered in this paper. Work on related systems, including the CIC of $[Ru(phen)_3]^{2+}$, is in progress.

Acknowledgment. We are grateful to Prof. Dr. E. J. Baerends for providing us with the electrostatic molecular potential data, to Prof. Dr. C. A. Reynolds for valuable discussion on MEP fitting, to Dr. J. D. Gale for making a prerelease version of his code GULP available, and to BIOSYM Technologies for making available to us both the INSIGHT and DISCOVER packages. J.B. would like to thank Prof. Dr. K.-J. Range for his constant support and the DFG for a postdoctoral fellowship.

Supporting Information Available: Figures 9–14, showing the remaining local minima, and tables of the potential parameters used (5 pages). Ordering information is given on any current masthead page.

IC950121D